Weierstraß-Institut
für Angewandte Analysis und Stochastik
Leibniz-Institut im Forschungsverbund Berlin e. V.

Preprint ISSN 0946 – 8633

Feel the heat: Nonlinear electrothermal feedback in Organic LEDs

Axel Fischer[1], Thomas Koprucki [2], Klaus Gärtner[2], Max L. Tietze[1],

Jacqueline Brückner[3], Björn Lüssem[1], Karl Leo[1],

Annegret Glitzky[2], Reinhard Scholz[1]

submitted: September 10, 2013

[1] Institut für Angewandte Photophysik (IAPP)
Technische Universität Dresden
George-Bähr-Straße 1
01069 Dresden, Germany

[2] Weierstraß-Institut
Mohrenstraße 39
10117 Berlin
Germany

[3] Fraunhofer COMEDD
Maria-Reiche-Str. 2
01109 Dresden
Germany

No. 1839
Berlin 2013

2010 *Mathematics Subject Classification.* 82D37, 80A20.

2008 *Physics and Astronomy Classification Scheme.* 81.05.Fb, 85.60.Jb, 72.80.Le.

Key words and phrases. Organic light emitting diodes, Joule self-heating, negative differential resistance, device temperature, luminance.

The work leading to these results has been received founding from the Deutsche Forschungsgemeinschaft (DFG) within the collaborative research center SFB 787 Semiconductor Nanophotonics (Th. Koprucki), DFG Research Center MATHEON under project D22 (A. Glitzky), by the European Communitys Seventh Framework Programme under Grant Agreement No. FP7-267995 — NUDEV— (A. Fischer), by the excellence cluster cfaed, and by the Free State of Saxony and the European Commission (EFRE) within the project Next-O-Light (100135204) (J. Brückner).

Edited by
Weierstraß-Institut für Angewandte Analysis und Stochastik (WIAS)
Leibniz-Institut im Forschungsverbund Berlin e. V.
Mohrenstraße 39
10117 Berlin
Germany

Fax: +49 30 20372-303
E-Mail: preprint@wias-berlin.de
World Wide Web: http://www.wias-berlin.de/

Abstract. For lighting applications, Organic light-emitting diodes (OLED) need much higher brightness than for displays, leading to self-heating. Due to the temperature-activated transport in organic semiconductors, this can result in brightness inhomogeneities and catastrophic failure. Here, we show that due to the strong electrothermal feedback of OLEDs, the common spatial current and voltage distribution is completely changed, requiring advanced device modeling and operation concepts. Our study clearly demonstrates the effect of negative differential resistance (NDR) in OLEDs induced by self-heating. As a consequence, for increasing voltage, regions with declining voltages are propagating through the device, and even more interestingly, a part of these regions show even decreasing currents, leading to strong local variation in luminance. The expected breakthrough of OLED lighting technology will require an improved price performance ratio, and the realization of modules with very high brightness but untainted appearance is considered to be an essential step into this direction. Thus, a deeper understanding of the control of electrothermal feedback will help to make OLEDs in lighting more competitive.

1. Introduction

Organic light-emitting diodes (OLED) are commercially successful and are used in high-end displays in mobile phones and TV applications. The advantages of this technology are low material costs, low processing temperatures, high luminous efficacy [1], and large area production. OLEDs are fabricated by depositing different functional layers in between two planar electrodes, typically called sandwich-type geometry [2]. The function of the layers include charge injection, charge transport, exciton recombination, or charge blocking barriers. White OLEDs have the potential for high quality lighting, but the respective products have not found their way into mass market yet [3]. In 2009, Reineke et al. realized a white OLED with 90 lm/W at a brightness of 1000 cd/m^2 [4]. OLED manufacturers have announced white light OLED tiles with a luminous efficacy of 80 lm/W and a homogeneous brightness of ca. 3000 cd/m^2 [5]. Despite this progress, for several applications e.g. general lighting the costs per module are still too high. For that reason, if OLED tiles would reach 5000 to 10000 cd/m^2, resulting in an overall better price to performance ratio, it would help to access a larger market.

OLEDs can indeed reach this luminance, but on large areas two main aspects prevent the realization. Firstly, the more transparent electrode has a rather high sheet resistance. This will lead to a voltage drop along this electrode, darkening the center of the panel with respect to the edges. This can be overcome by supporting the transparent electrode with a highly conductive mesh grid [6, 7, 8]. Secondly, Joule self-heating will appear at much lower brightness due to the large dimensions. Regions which heat up most strongly have an increased conductivity of the OLED layers so that these areas could become somewhat brighter. In the beginning, both effects can counteract each other, since they have an opposite influence onto the brightness in the center of the lighting panel. However, with rising temperature, OLED panels tend to show extreme brightness inhomogeneities. An improved heat conduction into the environment can help [9, 10, 11, 12, 13], but this would mean to relinquish well established procedures like fabrication on glass substrate or plastic foils.

The best solution would be to increase the luminous efficacy of the OLEDs as argued by Sasabe and Kido [14], leading to higher brightness, lower self-heating, and of course a more economic conversion of electrical power into light. However,

state-of-the-art OLEDs are already highly optimized, raising the question whether a further performance increase by a factor of 2-3 can be realized. Another approach is to accept the self-heating with the benefit that higher currents are driven, allowing to reach higher light output. Several publications show simulations of self-heating in OLEDs, and some of them consider electrothermal modeling, demonstrating that self-heating causes brightness inhomogeneities [15, 16, 17, 18, 19, 20], but the results do not describe the entire behavior as we will show in this work. To understand the prospects and limitations of self-heating, a description of the OLED at strong self-heating is required.

Recently, it has been revealed that organic semiconductors do essentially show the behavior of thermistor devices [21]. A thermistor is an electronic device with a strong temperature dependence of the conductivity, often described by an Arrhenius law

$$\sigma(T) = \sigma_0 \exp\left(\frac{B}{T}\right) , \tag{1}$$

where σ_0 is a reference conductivity, T is the temperature, and B is the temperature coefficient. In the case of organic semiconductors, $B < 0$ is a negative temperature coefficient (NTC), and thus the conductivity increases under rising temperature. If a constant voltage is applied, this can lead to a strong positive feedback loop between power dissipation and current flow, finally leading to a thermal runaway phenomenon in which an electronic device shows a switching from a rather low current density branch to a branch with a very high current density [22, 21]. Normally, this induces the destruction of the device by thermal breakdown. It is known that a thermistor can be stabilized by using a resistor in series, and thus bistability is suppressed [23]. However, at relevant currents, the thermistor will still enter into a region of negative differential resistance (NDR) which is the mathematical reason for the switching phenomena. As a consequence, NTC-thermistors have an "S"-shaped current-voltage (IV) characteristic. In OLEDs, as a representative for organic semiconductor devices, to the best of our knowledge such effects have not been demonstrated or they have just led to uncontrolled destruction of the devices [24]. One reason could be the fact that the transparent electrode introduces both a sheet resistance and an external series resistance, limiting the current and hiding a S-shaped behavior of the IV curve. Hence, the challenge consists in demonstrating the presence of an NDR effect induced by self-heating in OLEDs and to find out how the zero-dimensional thermistor model behaves in a spatial configuration where the lateral expansion of the active area is huge with respect to the thickness, the current has to flow through vertically. Due to the outcoupled light which is roughly proportional to the current flow, OLEDs would provide a perfect model system, allowing to study the effects in detail.

Here, we show that OLEDs under self-heating can enter an operation mode where NDR-regions with declining voltages are laterally expanding through the device and generate zones where both voltages and currents are "switched back". This highly interesting observation is a unique feature of a lateral thermistor array like an OLED decreasing the homogeneity of brightness. We present a simple, yet efficient technique to detect the presence of NDR-regions in a crossbar OLED test structure, as they are typically used in device development in order to investigate new layer stacks. An electrothermal network simulation is subsequently introduced, giving insight into the propagation of the NDR-regions and the switched-back regions in the device. Finally, our results are transferred to a large area OLED lighting panel, demonstrating the impact of the effect.

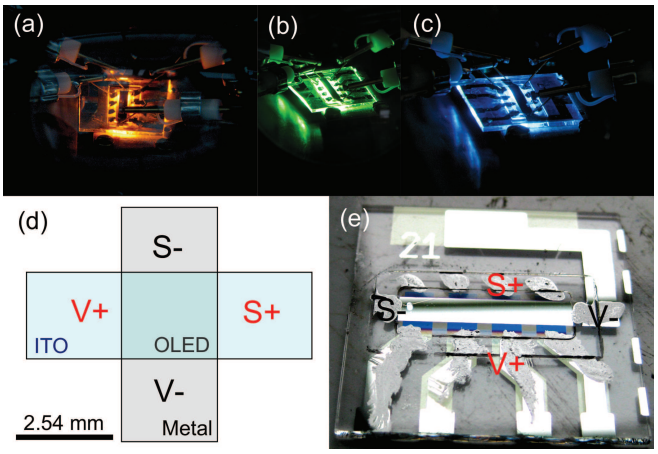

FIGURE 1. a)- c) Pictures of a red, green, and blue OLED during 4-wire crossbar measurement. d) Setup of the 4-wire crossbar measurement. The external voltage V is applied between $V+$ and $V-$. The contacts $S+$ and $S-$ are used to detect the voltage S at the backside of the device. e) Decapsulated sample after measurement. Liquid silver covers the contacts to minimize residual contact resistances.

2. RESULTS

2.1. **Improved setup: 4-wire crossbar measurements.** For measuring possible NDR-effects due to self-heating, we have created a new measurement setup, called 4-wire crossbar. Figure 1d visualizes this setup in a topview of an OLED crossbar structure. In an usual current-voltage measurement, the two different electrodes are contacted from a single side to apply a low (V-) and a high (V+) potential. Between these potentials, the total current I flows, realized by a current source. However, since electrodes overlap the active area, a second contact can be connected to each electrode to sense the potential which is present at the opposite side. For each electrode, independently whether the potential is low (S-) or high (S+), a sensing contact can be applied. The voltage S between both sensing contacts can be measured and compared to the originally applied voltage V between V- and V+. The idea of this setup is that whenever a NDR will appear in the device, problems arising in two terminal measurements can be avoided, including the impact of the series resistance of the ITO outside the active area or the fact that thermal runaway occurs which eventually destroys the device. However, with additional sensing contacts, it might be possible to detect the voltage decrease inside the device, since it is a typical feature of 4-wire measurements that a series resistance is excluded.

For measurement, we use standardized samples which are used for tracking purposes to continuously check processing quality (c. Appendix Fig. A.2). Similar OLED configurations have been published in Ref. [25, 26]. To realize a 4-wire crossbar measurement, encapsulation is removed in a glovebox while their current-voltage characteristics remain unchanged. All contacts are enhanced with silver liquid to ensure proper connection to the contact needles. A picture of a sample after measurement can be seen in Fig. 1e. The measurement performed during operation of a red, green, and blue OLED are shown in Fig. 1a-c.

The results are plotted in Fig. 2 for a current sweep from 1 mA until degradation appears, with 100 values per decade. First, we will concentrate onto the current

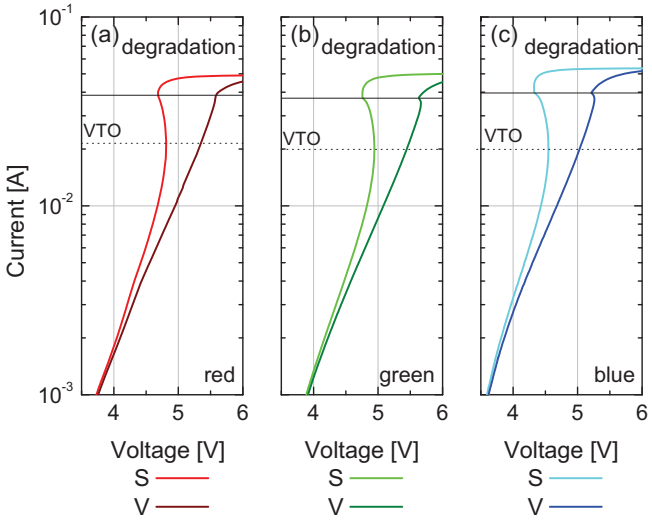

FIGURE 2. IV characteristics of the 4-wire crossbar measurement for a red, green, and blue OLED. The total current is plotted over the voltage V, to drive the current and the measured voltage S at the sensing contact. Starting with 20 mA voltages are decreasing with increasing current, indicating the NDR-effect. A dotted line denotes this voltage turnover (VTO). This happens before samples degrade due to overheat in the range between 35 mA and 40 mA, corresponding to device temperatures around 60 °C (s. Appendix Fig. A.3).

plotted over the applied voltage V. The corresponding data coincide with a normal 2-wire measurement. With rising voltages the current also rises until ca. 40 mA (solid black lines) are reached which will unavoidably lead to the degradation of the sample due to self-heating. Since these OLED layer structures become high-Ohmic while degrading, the applied voltage V rises caused by the constant current mode. Thus, the dissipated power increases and heats up the device until the degradation starts revealed by a kink in the IV curves. This point lies in a temperature range between 60 °C and 65 °C (s. Appendix Fig. A.3). Besides this, a 2-wire measurement of an OLED will not disclose any special effects.

Now, we will focus on currents plotted over the sensed voltage S. In contrast to the previous measurement, a qualitatively different result is obtained. Beginning from 1 mA, both types of curve deviate from each other, revealing the beginning of self-heating. Most interestingly, by reaching about 20 mA, the sensed contacts show a voltage turnover, clearly distinguishable to the onset of the degradation. By thermal imaging of an encapsulated sample we estimate an upper limit of the maximum temperature in the range of 45 °C (s. Appendix Fig. A.1). Furthermore, the stability and reversibility of the effect is checked by a well-defined forward and backward sweep (s. Appendix Fig. A.4). As a result, the 4-wire crossbar measurement clearly proves the presence of NDR due to self-heating, present in a red, a green, and a blue OLED. The capability to measure self-heating is further proven by the fact that a change of the thermal environment (s. Appendix Fig. A.6) shifts the voltage turnover, whereas the currents and voltages around 1 mA remain similar. Additionally, such a setup will also account for effects induced by a series resistance since it coincides with a normal 4-wire measurement if no self-heating is present.

2.2. **Electrothermal OLED simulations.** The voltage V and the voltage S differ under self-heating, and thus it is expected that the voltage within the device is not uniform anymore, leading to inhomogeneous current transport and heat dissipation. With the help of an electrothermal network simulation, we try to understand the processes taking place in the OLED. Therefore, a thermistor device [27] is modeled by a product ansatz of an isothermal power law current-voltage characteristic and an Arrhenius like conductivity-temperature law

$$I(V,T) = I_{\mathrm{ref}} \left(\frac{V}{V_{\mathrm{ref}}} \right)^{\alpha} \exp \left[-\frac{E_{\mathrm{act}}}{k_{\mathrm{B}}} \left(\frac{1}{T} - \frac{1}{T_{\mathrm{a}}} \right) \right], \tag{2}$$

where α is the exponent of the power law, T is the temperature, E_{act} is the activation energy of the conductivity, and T_{a} is the ambient temperature.

Comparison with the analytic solution proves the correct function for one thermistor in series with a resistor (s. Appendix Fig. B.7). An array ($m = 10 \times n = 10$) of thermistor devices now represents the active area and the current of each thermistor I_{ij} equals the charge flow through the OLED layer stack for a certain part of the active area. For simplicity, it is assumed that the metal electrode (cathode) of the OLED has such a low sheet resistance in comparison to the ITO (anode) that its influence can be neglected. Thus, all upper connections of the thermistor array are connected to each other. The anode is modeled by connecting all upper electrical contacts of the thermistor array via a network of resistors corresponding to a sheet resistance of $26.5\,\Omega$. Furthermore, the thermistor array is coupled to a thermal network, modeling both the glass substrate and the heat transport into the environment. In this thermal network, a resistor corresponds to a thermal resistance, a voltage represents a temperature difference, and a current represents a heat flow. The thermal network is a 3D resistor network and includes regions outside the electrically active area. Detailed network schemes and further informations can be found within the Appendix in Fig. C.11, C.12, and D.13. Besides heat generated by the thermistor devices, the simulation incorporates voltage drops along the anode, producing a further heat source fed into thermal network.

For a comparison of experiment and simulation, further 4-wire crossbar measurements are performed on a green OLED, mounted onto a copper block. The results are shown in Fig. 3.

The power law describing the isothermal current-voltage characteristic of the OLED is easily fitted by defining a reference point where no self-heating occurs. In our example, this is $I_{\mathrm{ref}} = 1\,\mathrm{mA}$ and $V_{\mathrm{ref}} = 3.942\,\mathrm{V}$ so that the IV curve of the total thermistor array is fixed to this point and the correct increase can be tuned by adjusting the exponent of the power law to $\alpha = 8.7$. The fact that a part of the applied power is coupled out as light is considered by reducing the generated heat by 20%. For simplicity, this value is kept constant.

The thermal system of the OLED can be described by a heat flow downwards into the glass substrate and upwards into the nitrogen atmosphere. A lateral flow to the substrate given by the thin electrodes or the organic molecular layers is neglected (c. Ref. [28]). The use of a simplified resistor network to model the heat transfer requires a well-defined and easy to describe thermal system. Therefore, we fix the glass substrate to a copper block via heat sink paste to ensure proper thermal contact. The heat transfer from the OLED into the glass substrate and from the glass substrate into the copper block is supposed as ideal. Since the large copper block has a high heat conductivity ($400\,\mathrm{W/m/K}$), its temperature can be assumed to correspond to the ambient temperature T_{a}. Thus, the limiting factor for heat transport is the thermal conductivity of glass, chosen to be $1.8\,\mathrm{W/m/K}$. In the simulation, a variation of this parameter shifts the point of the voltage

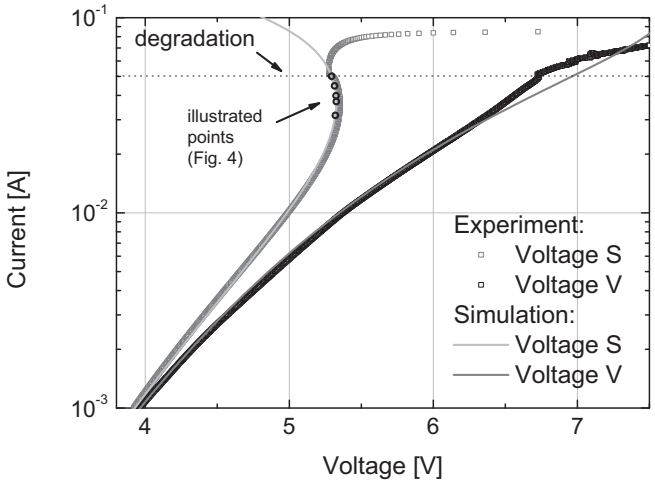

FIGURE 3. Simulated and measured IV characteristics of the 4-wire crossbar experiment on the green OLED. The simulation of the sensing voltage S reproduces the experiment up to the point where the device starts to degrade. Small black circles indicate the currents at which simulated current density and temperature are presented in Fig. 4.

turnover to higher or lower currents along the normally measured curve. For the heat flow upwards from the OLED to air, we use a rather overestimated coefficient of $10\,\mathrm{W/m^2/K}$, anyhow still realizing a minor heat flow with respect to that realized by the glass substrate and the copper block.

Besides modeling the thermal environment, the most important parameter of the system is the activation energy E_{act} of the OLED, used in Eq. (2). This parameter influences the shape of the sensed current-voltage curve, leading to a stronger curvature with increasing activation energy. By using $E_{\mathrm{act}} = 25\,k_{\mathrm{B}}T_{\mathrm{a}}$, a good agreement between experiment and simulation is achieved. Within the Appendix (cf. Fig. A.3), temperature dependent IV measurements reveal activation energies between $13\,k_{\mathrm{B}}T_{\mathrm{a}}$ and $34\,k_{\mathrm{B}}T_{\mathrm{a}}$ for different voltages at temperatures from -30 °C to 30 °C. At higher temperatures, extraction of suitable values is influenced by self-heating, but most disturbingly, series resistances of the electrodes and the setup will limit the current flow, decreasing the real voltage drop of the OLED, resulting in underestimated activation energies. More details about implementation of the parameters can be found in the Appendix. Although, this model of thermistors, electrical resistors, and thermal resistors is quite simple, it accounts for all qualitative aspects of the system described above, and furthermore it allows to reproduce the experimental results, as visualized in Fig. 3. Degradation effects above 50 mA are not incorporated and no agreement can be achieved above this value.

A closer look into the simulated distribution of currents and temperature is given in Fig. 4 for five different values of the total device currents as shown in Fig. 3. Each picture shows the active area of the OLED sample. The electrodes are connected as visualized in Fig. 1d, meaning that the current essentially flows from the left side (ITO) through the OLED stack and leaves at the bottom side via the metal electrode. With increase of the total current, the current density in the device will strongly rise in the left region of the active area while at the opposite side the current seems to change less. A similar behavior can be seen for the temperature increase which appears more widened but still is mainly located close to the left

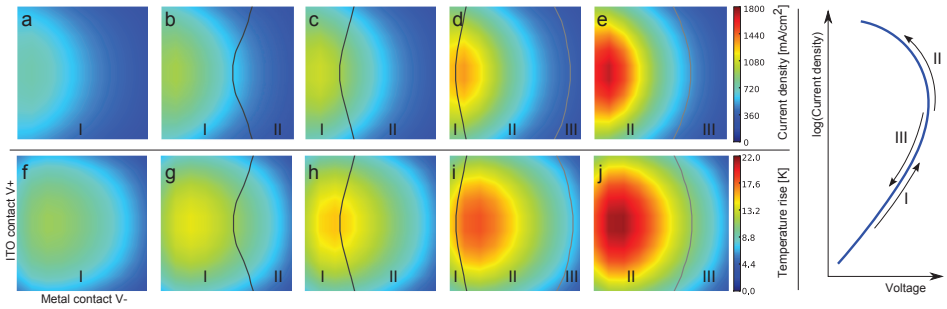

FIGURE 4. Simulated distributions of current density a)-e) and temperature rise f) - j) for total currents of 31.6 mA, 37.2 mA, 39.8 mA, 44.7 mA and 50.1 mA as marked in Fig 3. The schematic diagram shows the three operation regimes in a current-voltage plot of a thermistor. Normal (I): Increasing current density and voltage. S-NDR (II): Increasing Current density while voltage decreases. Switched-back (III): Both, current density and voltage decreases. The schematic IV curve visualizes the different operation modes for each thermistor.

voltage / current	$\frac{dV_{ij}}{dV} > 0$	$\frac{dV_{ij}}{dV} < 0$
$\frac{dI_{ij}}{dI} > 0$	$\frac{dV_{ij}}{dI} > 0$ normal (I)	$\frac{dV_{ij}}{dI} < 0$ S-NDR (II)
$\frac{dI_{ij}}{dI} < 0$	$\frac{dV_{ij}}{dI} < 0$ N-NDR (not present)	$\frac{dV_{ij}}{dI} > 0$ switched-back (III)

FIGURE 5. The table visualizes the four different types of differential resistance. In a thermistor array, three of them are possible: normal (I), S-NDR (II), and switched-back (III).

edge of the active area. Significant is that both current density and temperature rise tend to consolidate more and more towards the left region whereas close to the right edge they remain nearly unaffected by changes of the total applied current or voltage.

From the fact that declining voltages have been obtained in Fig. 2, it is essential to investigate the local current I_{ij} and the local voltage V_{ij} in terms of NDR. Therefore, we define the local differential resistance

$$R_{\mathrm{diff,ij}} = \frac{dV_{ij}}{dI_{ij}} \tag{3}$$

as the differential of the local voltages and currents across the OLED layers between top and bottom contact. To indicate if $R_{\mathrm{diff,ij}} = 0$, a dark grey line is plotted in Fig. 4, separating region I and region II. Region I behaves normal, having increasing currents while voltages are rising. In contrast, region II has a local NDR, and thus currents are rising under decreasing voltages. It is obvious that regions of NDR are shifting from the right to the left with the increase of the total device current. They appear first with the occurrence of the voltage turnover of the sensed voltage S in the 4-wire crossbar measurement.

However, by reaching a certain current level, a new region III enters into the device from the right. Surprising to us, this region has once more a positive differential resistance, similar to the normally behaving region I. To understand how this phenomena can be understood, the differential resistance has to be analyzed in more detail. In Fig. 5, a table of four possible configurations is shown. For example, the local change in voltage is characterized by dV_{ij}/dV, and analogously for currents, dI_{ij}/dI characterizes the local change in current. In a normal operation mode, currents and voltages increase at the same time with their external counterparts, while in a "S"-shaped NDR (S-NDR) region, currents will increase for decreasing externally applied voltages V. A very interesting configuration is realized when local currents and voltages decline at the same time even though externally applied currents and voltages increase further. By comparison of the individual terms within the simulation result, it is found that in region III the OLED indeed shows such a strange behavior. It can be fully understood if one reminds the decreasing local voltages in region II. Due to the fact that the ITO electrode is contacted from the left side, OLED regions at the opposite side might not generate enough power dissipation to heat up and reach a NDR. Then they are supplied with the reduced voltage after the lateral passage of the NDR region (II). Since this region has declining voltages, in region III the OLED layer stack does only "notice" a declining voltage and consequently the current density is switched back. To give a simpler picture of that mechanisms, we provide calculations of three parallel thermistors coupled by series resistors, compare Fig. B.8 and B.9 in the Appendix. There it is shown that in a one-dimensional thermistor chain, all thermistors behind the first one are instantly switched back if no thermal coupling exists between them. If thermal coupling is incorporated, due to the heat exchange between individual thermistors, the abrupt switch back is replaced by a smoother transition similar to the simulations of the two dimensional thermistor array presented in Fig. 4.

The fourth configuration in Fig. 5 is a decrease of the current accompanied by increasing voltages. This operation mode would correspond to a "N"-shaped NDR and is not present in this system due to the nature of the self-heating phenomena. The operation of region I, II, and III is further visualized in the schematic IV curve of Fig. 4. Please note, however, that due to the thermal coupling, every thermistor in the network has its own dependence $I(V,T)$ on voltage and temperature.

2.3. **Large active area lighting panel.** Previous crossbar measurements show that the distribution of current becomes strongly inhomogeneous when the NDR effect arises. It remains an open question whether these effects have also impact onto OLED applications like lighting.

For that reason, we investigate the luminance distribution of an opaque Tabola lighting panel (produced by Fraunhofer COMEDD, Dresden) with an active area of $15\,\mathrm{cm} \times 7.5\,\mathrm{cm}$. This tile size is representative for present-day OLED lighting applications. The metallic electrode has its contacts to the power supply at the four corners and the ITO electrode is contacted via a metallic frame all around the active area. Please find more details on the Tabola within the Appendix. The centered cross-section of the luminance for the longer device width is shown in Fig. 6a. While these lighting panel have a high brightness homogeneity around $1000\,\mathrm{cd/m^2}$ (ca. 200-300 mA), and are still acceptable for $2000\,\mathrm{cd/m^2}$, with increasing current, luminance will only increase at the edges, but the center position shows a saturation of luminance. One might expect the central region to be hottest and thus degradation processes will take place there, but this is not the case as revealed in Fig. 6b. At the highest currents, the temperature distribution shows two maxima which are located close to the edges. This might seem surprising, since the center of the lighting panel is supposed to face the worst conditions to conduct away the

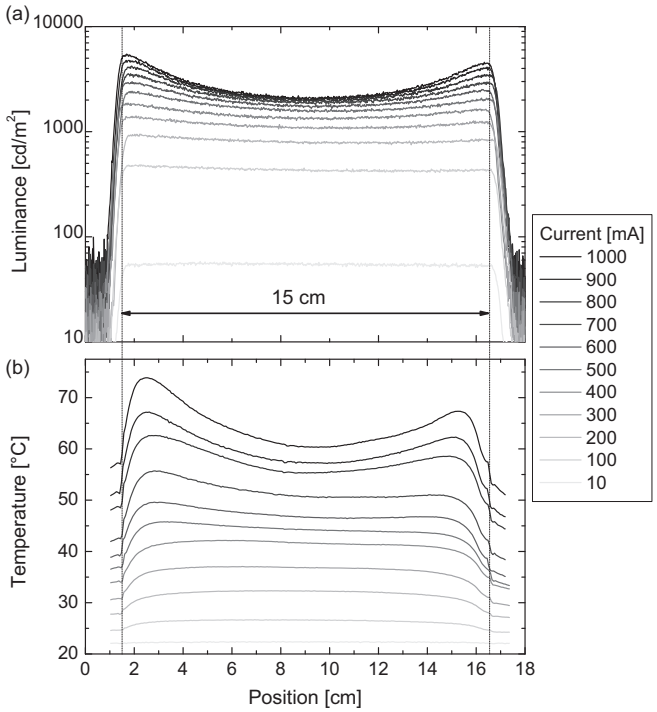

FIGURE 6. Measured a) luminance and b) temperature profiles of a warm white lighting panel with the dimensions 15 cm × 7.5 cm. At 1000 cd/m^2, the homogeneity is alright, but it drastically changes under self-heating. Starting around 500 mA the luminance in the center of the device saturates and hardly exceeds 2000 cd/m^2, whereas the luminance in the maximum region still linearly increases (s. Appendix). We exclude a degradation at the center of the lighting panel, since highest temperatures should rather effect the outer regions. Consequently, the reduction of luminance is related to the formation of a switched-back region which further implies already the existence of NDR-regions in the device at lower currents.

heat. However, the power dissipation close to the edges strongly rises with respect to the central region. In Fig. 7a, experimental values of the luminance vs. total device current are presented for a position at the edge and at the center for the cross-section, shown in Fig. 6a. It becomes obvious that both curves begin to split shortly before 2000 cd/m^2 are reached. In this double logarithmic plot the luminance at the center does hardly increase anymore while the luminance at the edge position seem to increase even slightly super linearly. If we consider the typical efficiency roll-off [29, 30, 31, 32] of an OLED at high current densities, a weaker increase of luminance over current is expected.

To clarify this, we adopt the network model, described above, onto the geometry of the Tabola lighting panel. Please find further details within the Appendix. The fully metallic electrode is assumed to have a negligible sheet resistance and for the bottom ITO electrode, responsible for light outcoupling through the substrate, a sheet resistance of 8 Ω is used as measured with a common 4-point probe setup. Again, the isothermal current-voltage characteristic of the device is fitted by a power law applied to a point ($I_{\mathrm{ref}} = 10\,\mathrm{mA}$, $V_{\mathrm{ref}} = 7.2\,\mathrm{V}$) where no self-heating appears

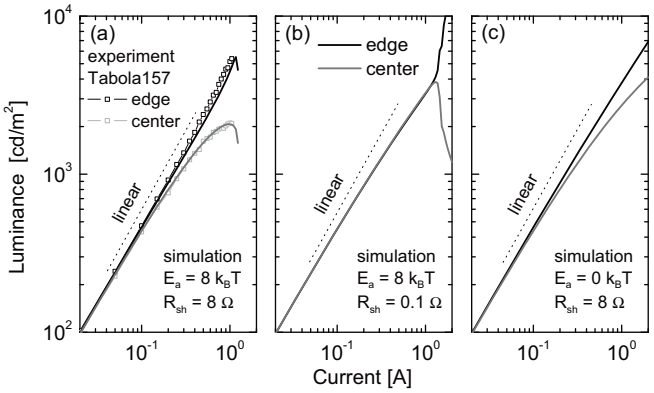

FIGURE 7. Comparison between experiment and simulation for the luminance at the center and the midpoint of the shorter edge. a) Measured luminance at the edge and at the center of the lighting panel vs. simulation results. Up to a current of 1 A, a strong effect of sample degradation can be excluded. b) Simulation with reduced sheet resistance. c) Simulation with no activation energy.

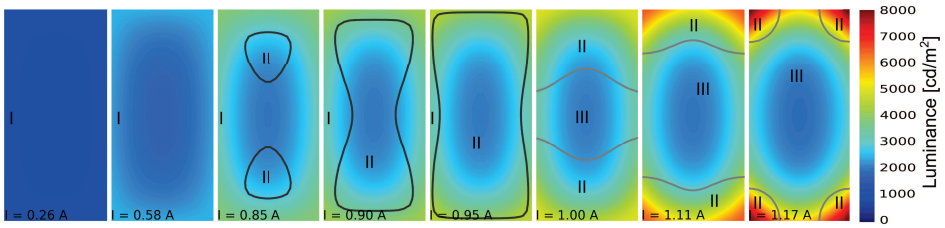

FIGURE 8. Each picture corresponds to a simulated luminance distribution of a 15 cm × 7.5 cm large Tabola lighting panel. At 0.26 A, the luminance of around 1000 cd/m^2 is very homogenous, changing when the current is increased twice. Around 0.85 A, first regions with local NDR (II) appear. Around 1 A, all normal regions (I) have vanished and the first switched-back regions (III) appear. Dark grey lines separate regions I and II whereas bright grey lines separate regions II and III.

and high current homogeneity can be assumed. To account for the current efficiency roll-off, we fit this value over various currents where a homogeneous brightness is given (s. Appendix Fig. E.16). With the help of the analytical expression, luminance values are calculated from the simulated current density. However, for the reason of simplicity, the generated heat is still reduced by a constant value of 20% due to light outcoupling. The most important parameter of the simulation is the activation energy chosen to be $8\,k_\mathrm{B}T_\mathrm{a}$. This value, significantly below the activation energies necessary to simulate the small active area OLEDs in the section above, can be justified by the fact that the white light of the Tabola lighting panel is created by multiple color OLED layer stacks connected in series.

Under these reasonable assumptions, the experimental values in Fig. 7a are reproduced over the measured current range. For comparison, a simulation with a small sheet resistance of the ITO electrode and with no activation energy assumed

are shown in Fig. 7b and c, respectively. In both cases, the simulation behaves quite differently.

The saturation of brightness in the center can be understood by the visualization of the simulated luminance and the occurrence of the normal region (I), the NDR-region (II) and the switched-back region (III) in Fig. 8. Due to the rectangular geometry and the anode contacted from all sides, first NDR-regions appear around 0.85 A inside the active area at two different locations. After they have merged, this region is growing towards the edges. At around 1 A, a switched-back region appears first in the center of the lighting panel and expands subsequently to the nearest edges. This is the reason why the simulation predicts a saturation accompanied by a return of the luminance in the central region. With that knowledge we estimate that the central region of the Tabola lighting panel has reached or is shortly before entering the switched-back operation mode at the highest measured currents, and it is likely that larger parts of the device already show local NDR. However, with the further expansion of the switched-back region, the current distribution of the device will become unstable due to the fact that any additional rise of the total current will lead to an extreme current increase in the residual NDR-regions, located at the corners, enhanced by the current reduction in the switched-back regions. This explains why the luminance at the edges increases linearly or slightly stronger with current, even though current efficiency roll-off takes place.

We would like to mention that the simulation reveals a switching phenomenon into a more stable electrothermal configuration (not shown) when the total current exceeds 1.24 A (c. Fig 7a). It will be the topic of further investigations to study these aspects in more detail.

3. Conclusion

We show that irrespective of the device area, OLEDs display such a strong electrothermal feedback that negative differential resistance will occur. By using 4-wire crossbar measurements, this has been clearly proven by experiment. This technique is ideal to investigate the influence of several parameters like activation energy of the OLED, sheet resistance of the electrodes, or simply the series resistance of the setup. Further electric network simulation demonstrate that an OLED can essentially be understood as a two dimensional array of temperature activated thermistor devices. Upon self-heating, regions with local NDR will enter. As a further consequence, these regions are able to switch back regions located at a larger distance from the contacts. Thus, central regions or regions far away from the edges show a saturation or even a decrease in currents, even though the total current and voltage applied to the device are still increasing. This explains the dramatic increase of brightness inhomogeneities in OLED lighting panels when self-heating occurs in a pronounced manner. Our results are able to explain the most fundamental processes taking place in OLED devices under self-heating and can be adapted to similar thin film devices. In the future, simulations based on temperature-activated charge transport are expected to provide a deeper insight into the limitations of OLED lighting panels and applications. Besides helping to increase the efficiency of OLED, it will be of interest to investigate the origin of the activation energy. If it can be decreased, device function at elevated currents could guarantee higher brightness combined with untainted appearance of the OLED tiles and reducing the risk of electrothermal instabilities or switching phenomena.

4. Experimental section

OLEDs for 4-wire crossbar measurements are fabricated by thermal vapor deposition in high vacuum. After cleaning of the prestructured ITO-glass substrates, a p-doped/intrinsic/n-doped layer configuration is realized, using 30 nm MeO-TPD:F6TCNNQ (2wt%), 10 nm NPB, a ca. 20 nm thick emitter system, 10 nm BAlq2, 30 nm BPhen:Cs (ratio: 1:1). F6TCNNQ is purchased from Novaled AG (Dresden, Germany). 100 nm Al realize the top electrode. For the emitter system, 20 nm MADN:TBPe (1.5wt%) (blue), 6 nm TCTA:Ir(ppy)3 (8wt%) and 12 nm TPBI:Ir(ppy)3 (8wt%) (green), 20 nm NPB:Ir(MDQ)$_2$(acac) (10wt%) (red) are used. The glass substrate has a size of 2.54 cm in square and a thickness of 1.1 mm. The active area is approximately 2.54 mm^2. 4-wire crossbar measurements are carried out with two source-measuring units Keithley 2400 controlled by a home built software. Network simulations are made by the freely available program LTSpice IV (Linear Technology) and a self-made circuit generator script. Results are evaluated with a self-made program using matplotlib for plotting the data. The simulation results are interpolated (contourf-function, linear interpolation) which does not change the value range or the local occurrence of NDR-regions. Temperature and luminance measurements are done by an IR camera VarioTHERM head II (company: JENOPTIK AG) calibrated with a thermo sensor PT1000 and a video photometer PR-905 from PhotoResearch Inc. The opaque Tabola lighting panel is fabricated at Fraunhofer COMEDD (Dresden, Germany) and uses a 3-unit-stacked architecture based on a fluorescent blue, phosphorescent green and phosphorescent orange unit.

Acknowledgment

The authors thank Simone Hofmann and Caroline Murawski for discussions and help with the measurement setup. This work was financed by the European Communitys Seventh Framework Programme under Grant Agreement No. FP7-267995 (NUDEV) (A.F.). Support from the excellence cluster cfaed is gratefully acknowledged. This work received funding from the Deutsche Forschungsgemeinschaft (DFG) within the DFG Research Center MATHEON under project D22 (A.G.) and the DFG CRC 787 "Semiconductor Nanophotonics" (T.K.) Part of this work was funded with support from the Free State of Saxony and the European Commission (EFRE) within the project Next-O-Light (100135204) (J.B.).

Appendix A. Information about OLEDs with small active area for 4-wire crossbar measurements

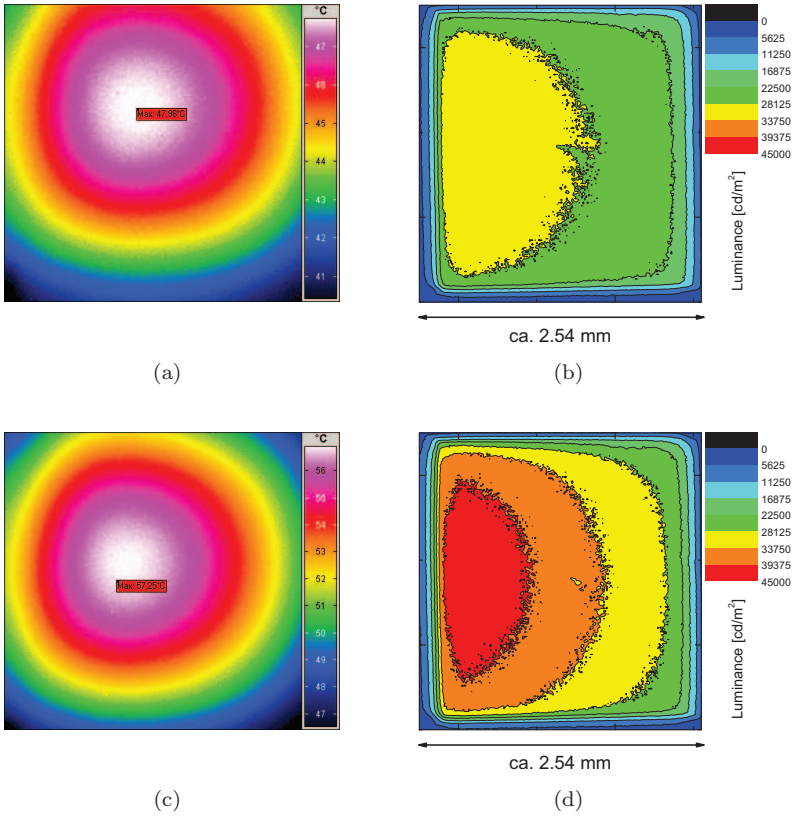

Figure A.1. Temperature (left, a, c) and luminance (right, b, d) imaging for a red encapsulated OLED a,c) at 20 mA; b,d) at 30 mA. The ITO electrode is horizontally aligned, and contacted from the left, whereas the metal electrode is vertically aligned, contacted from the bottom. Since the symmetry axis of the luminance pictures is a horizontal line through the center, it can be assumed that the metal electrode is much more conductive than the ITO electrode so that the sheet resistance of the metal electrode can be neglected in the simulation. The size of the pictures agrees with the active area. Thermal imaged samples are slightly shifted upwards to show the temperature decay. The maximum temperature rise at a) 20 mA is around 25 K and in c) a maximum temperature rise of ca. 33 K, is reached at 30 mA. It can be assumed that the samples already have regions with NDR since they are expected to enter this regime at a current of around 20 mA (c. Fig. A.6). The brightest areas are concentrated at the left side, whereas at the right side the luminance changes little with increasing current.

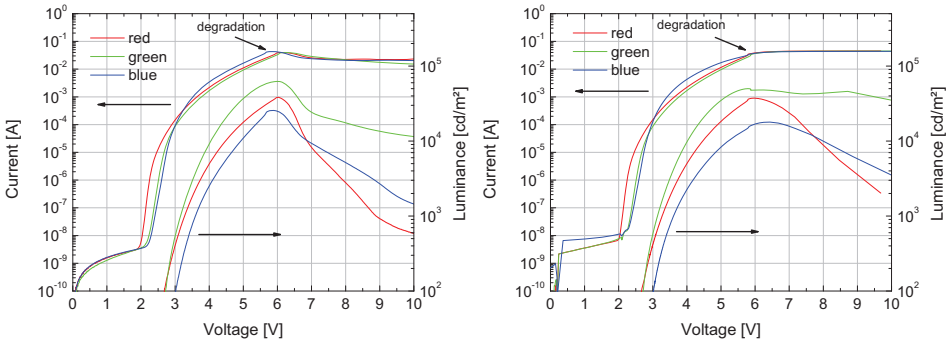

FIGURE A.2. Current and luminance over voltage for the red, green, and blue OLEDs used for 4-wire crossbar measurements. Samples are encapsulated and measured in normal two-terminal measurement with a) constant voltage given or b) constant current given for each measurement point. Depending on these measurement modes, different behavior can be observed after degradation has started. Since samples get high-Ohmic, the current will decrease in the constant voltage mode, whereas in a constant current mode the degradation is accelerated by a permanent increase in voltage and dissipating power. In this two-terminal measurement, no NDR-effect is observed. However, from the 4-wire crossbar measurement, it is known that OLEDs reach the NDR already before degradation starts. Luminance is measured with a calibrated photodiode, measuring the light output of the whole active area. The corresponding curves show no significant feature which can be unambiguously identified with NDR, shortly before degradation starts.

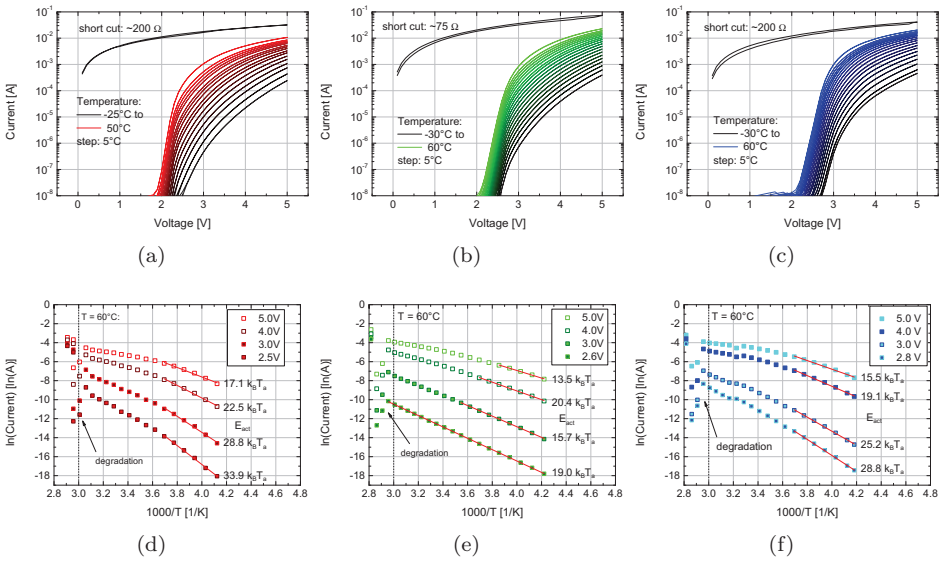

FIGURE A.3. Temperature dependent current-voltage measurements for a) red, b) green, and c) blue OLED. At various voltages the current is plotted in an Arrhenius plot over inverse temperature to extract the activation energies for d) red, e) green and f) blue OLED. After degradation, the samples finally show a short cut with a residual series resistance of around 75 Ω to 200 Ω, given by the setup and the resistance of the ITO electrodes. Thus, at high currents it can be expected that the correct temperature dependence is influenced by this series resistance so that the values for activation energies will be underestimated. However, activation energies determined at rather low temperatures are in the range between $15\,k_\mathrm{B}T_\mathrm{a}$ to $35\,k_\mathrm{B}T_\mathrm{a}$. In the temperature range around 60 °C, sample degradation due to overheating starts.

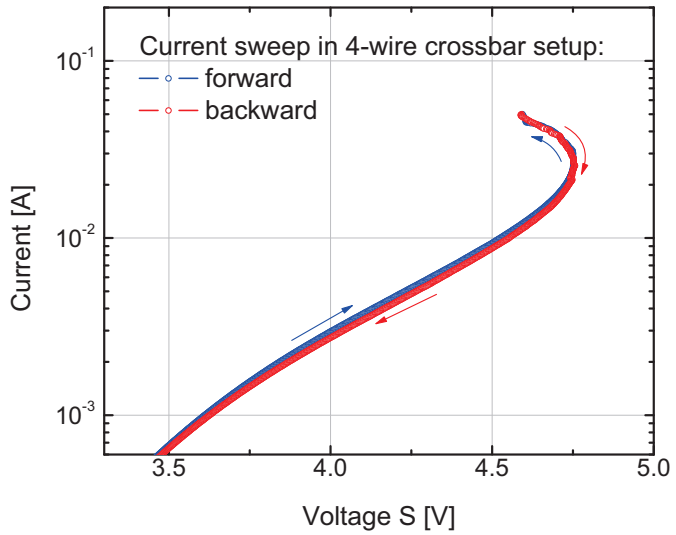

FIGURE A.4. Forward and backward sweep of a blue OLED. The highest current point is set to a value shortly before the degradation starts. Thus, it is possible to show that the voltage turnover is no effect of degradation or irreversible changes in the sample. This means that NDR regions occur within the device under normal operation without destruction of the functional layers.

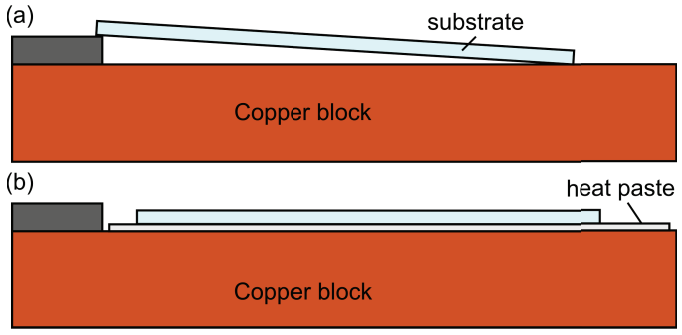

FIGURE A.5. Decapsulated samples are measured in a nitrogen atmosphere in two configurations: a) the substrate has an air slit to the underlying copper block and b) the substrate is directly mounted onto the copper block using heat paste to ensure proper thermal contact.

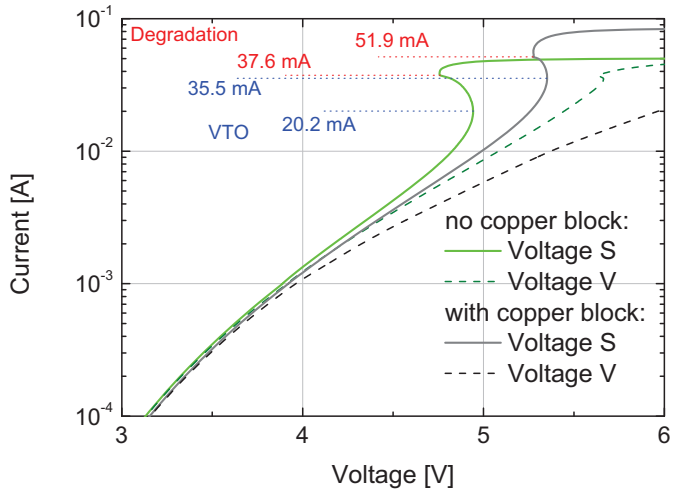

FIGURE A.6. Comparison between different thermal environments as explained in Fig. A.5. By using a copper block, both the point of the first voltage turnover (VTO) and the starting point of the degradation shift to higher current values, indicating an improved heat transfer. Measurement without contact to a copper block shows a VTO around 20 mA. For devices with capsulation shown in Fig A.1, the heat transfer should be even worse than for the measurement shown here. Therefore, it can be assumed that thermal and luminance images are taken under the presence of NDR-regions.

Appendix B. Description of a simplified network model

The network model is solved by the freely available software LTSpice IV (Linear Technology). It is a simulation program with integrated circuit emphasis (SPICE). For modeling, we define a thermistor device as published by Keskin [27] with the further implementation of a power law for the isothermal current-voltage characteristic of the thermistor. The power law is defined by a reference point (I_{ref}, V_{ref} which must be a point on the isothermal IV curve, and an exponent α. The thermistor model consists of two parts: An electrical part which defines the current-voltage characteristic with an Arrhenius-like temperature dependence of the conductivity, and a thermal part which accounts for a thermal heat flow where the electrical power dissipation acts as the heat source. In this thermal part, the potential difference necessary to conduct the heat flow into an externally connected thermal network corresponds to a temperature. Both parts of the thermistor model are in a feedback loop. The electrical part defines a dissipation power which is in turn used as a heat source by the thermal part to create a temperature. The resulting temperature increases the electrical conductivity within the electrical part.

To verify the thermistor model, we simulate a series connection of a thermistor and a resistor. For this simple circuit, an analytical solution can be derived [21]. In Fig. B.7, the SPICE model exactly reproduces the analytical solution for corresponding values of the resistor in series. Thus, the SPICE simulation is able to automatically reproduce the correct "S"-shaped self-consistent current-voltage characteristic under self-heating.

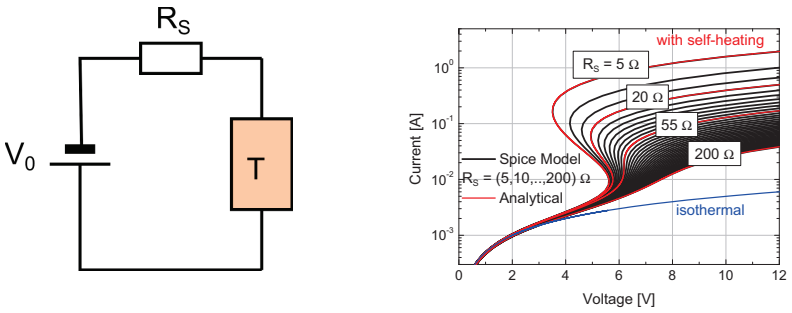

(a) (b)

Figure B.7. a) Circuit of a thermistor and a resistor in series. b) The SPICE model of the thermistor perfectly matches the analytical solution for corresponding resistor values. The blue line represents the current-voltage characteristic of an isothermal thermistor or a thermistor with no activation energy. For the analytical solution, please compare Ref. [21].

Now, it is possible to extend the circuit to three parallel thermistors with series resistive coupling as shown in Fig. B.8. This configuration is the most simple one-dimensional analog to the simulation of the 4-wire crossbar presented in the publication. Simulation results are shown in Fig. B.9 for the following parameters: The reference point of the power law like isothermal current-voltage characteristic is set to $I_{\mathrm{ref}} = 1\,\mathrm{mA}$ and $V_{\mathrm{ref}} = 3.9\,\mathrm{V}$ with the current equally distributed to all three thermistor devices. The exponent of the power law is 8. The series resistor have a resistance of $R_{\mathrm{S}} = 100\,\Omega$ and the resistors, representing the sheet resistance, have a resistance of $R_{\mathrm{sh}} = 100\,\Omega$. The thermal resistance for each thermistor is chosen to be $R_{\mathrm{th}} = 1000\,\mathrm{K/W}$. If no thermal coupling is assumed (R_{coup} is infinity), all

thermistor show a voltage return (c. Fig. B.9c), but only the first thermistor in the chain has increasing currents over the whole range of applied voltages (c. Fig. B.9a). In this case, most of the current flows through the thermistor T1 next to the voltage supply. In Fig. B.9e, the respective current-voltage characteristics for each of the thermistors is shown. While the first thermistor shows the typical S-NDR behavior, the remaining thermistors reach a maximum current and then return back on their IV curves because they are switched back by the decreasing voltage drop over the first thermistor which is passed to next thermistors via the connecting resistors.

The situation changes if a thermal coupling of $R_{\mathrm{coup}} = 1000\,\mathrm{K/W}$ is integrated into the electrothermal circuit. Now, the first thermistor will still have the highest currents, but due to the heat exchange between the thermistor devices, the thermistors T2 and T3 can be heated up by the strong power dissipation of the first thermistor T1 and thus reach a higher conductivity. In that configuration, thermistors T2 and T3 can have increasing currents although the voltage drop is decreasing. Even though the voltage drop over T2 is reduced by T1, the higher temperature at T2 produced by the power dissipation of T1 can still result in increasing currents across T2. In Fig. B.9b, thermistor T2 has now increasing currents over the whole range of externally applied voltages. A further feature is that every thermistor reaches its maximum voltage drop at different externally applied voltages as visualized in Fig. B.9d. And finally, it can be seen that the thermal coupling of the thermistors changes the current-voltage characteristic of each thermistor completely (c. Fig. B.9f). If the thermistor T3 switches back, it does not return along the same IV curve. This can be explained by the fact that due to heating by neighboring thermistor devices, the individual thermistors can have an increased temperature even if the device itself does not yet show substantial self-heating.

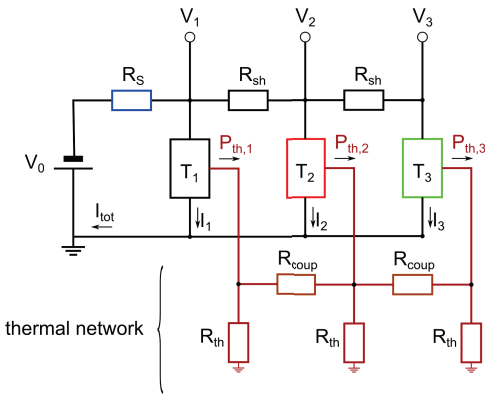

FIGURE B.8. Simplified SPICE circuit with three thermistors (T1, T2, T3) in parallel. They are electrically connected to each other by two resistors R_{sh}, representing the sheet resistance. The series resistor with the resistance $R_{\mathrm{S}} \times 2n$ connects the circuit to the power supply with the applied voltage V_0. The voltages dropping over the thermistors are denoted by V_1, V_2, and V_3, respectively. Each thermistor is connected to a resistor R_{th}, representing the thermal resistance of each thermistor. Via the resistors R_{coup}, the thermistors can be coupled thermally.

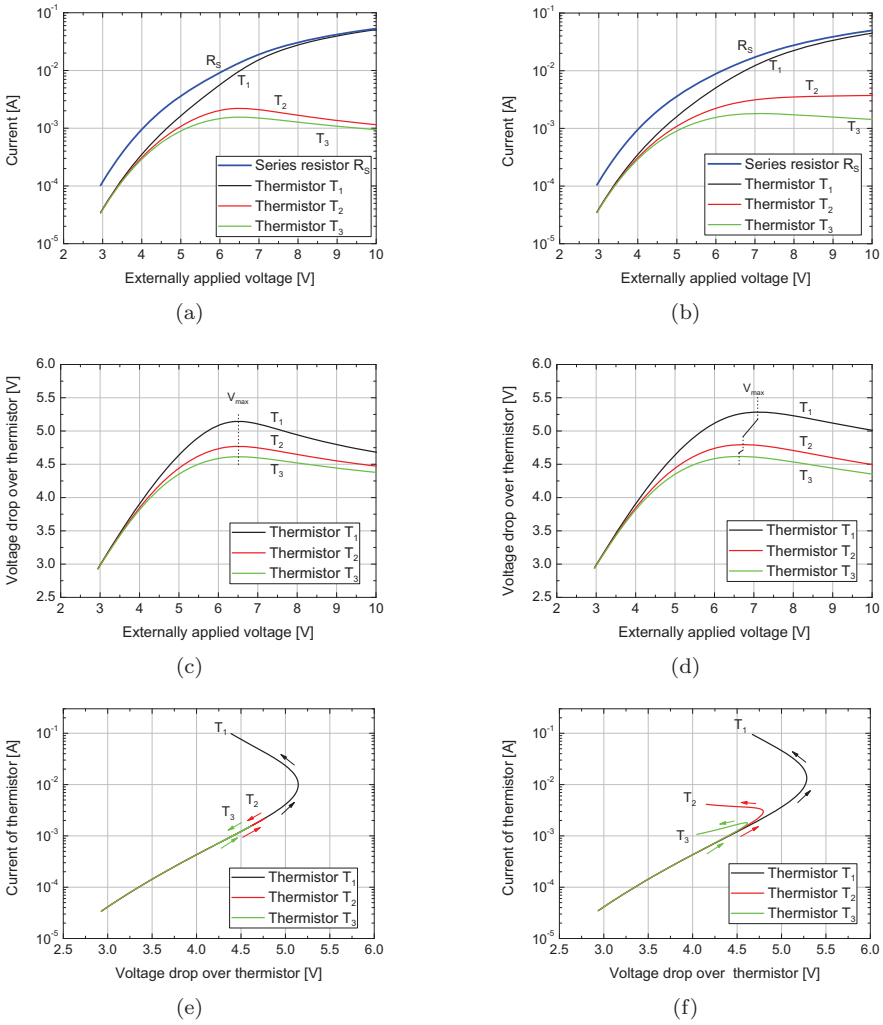

FIGURE B.9. Simulation results for the circuit presented in Fig. B.8. a), c) and e) Circuit without any thermal coupling between the thermistors ($R_{\mathrm{coup}} = \infty$). b), d) and f) Thermal coupling with $R_{\mathrm{coup}} = 1000\,\mathrm{K/W}$.

APPENDIX C. NETWORK MODEL FOR SIMULATION OF 4-WIRE CROSSBAR MEASUREMENT

The functional layers of the OLED are simulated as a two-dimensional array ($n = 5 \times m = 10$) of thermistor devices and the lateral electric conductivity of the OLED layers is neglected due to the much larger conductivity of the ITO. Every thermistor represents the vertical current flow through the OLED for a certain discretization area and is connected to an electrical grid used for the simulation of the ITO electrode as shown in Fig. C.10. In that way, all thermistors are connected to their nearest neighbors by a resistor representing the sheet resistance. Due to the quadratic grid, the value of the resistor equals exactly the value of the sheet resistance, chosen to be $R_{\mathrm{sh}} = 26.5\,\Omega$. The grid is connected to the power supply with the voltage $V+$ as well as to the contact for the sensing potential $S+$ via resistors with a value of $R_{\mathrm{S}} \times 2n$. The series resistance is set to $R_{\mathrm{S}} = 25\,\Omega$. On

the other side, the connection of the thermistor to the metallic electrode is set to a common potential because the sheet resistance of the metallic electrode is much smaller than that of the ITO electrode, as argued in Fig. A.1. As a consequence, the solution of the problem cannot anymore depend on the geometry of the metallic electrode and thus must be symmetric to the symmetry axis of the ITO electrode in that crossbar architecture. Therefore, the simulation of one half of the ITO electrode is sufficient to compute the whole simulation by reflecting the result at the symmetry axis. This procedure can reduce the computation time which is helpful since no automatic fit function is available and finding parameters is done step by step. However, one must ensure that the network model prevents any current or heat flow perpendicular to the symmetry axis of the ITO electrode to fulfill the boundary condition. The final result is then represented by a thermistor array of 10×10 devices. Although these are only 100 thermistors, describing the OLED, their number is sufficiently high to qualitatively reproduce the experimental results.

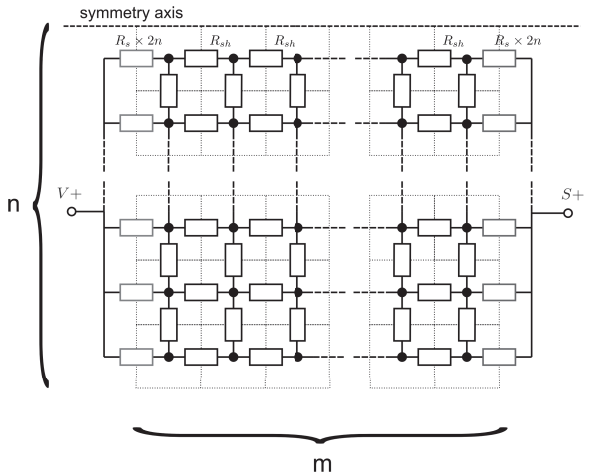

FIGURE C.10. Plane view of the electrical network used in the SPICE simulation representing the 4-wire crossbar measurement. Due to the symmetry of the setup (assuming no resistance of the metal), one half of the device is simulated and results are reflected afterwords at the symmetry axis. Big dots represent the connection to one thermistor. Additional series resistors to the sensing contact (S+) are inserted to not short circuit the thermistor devices at the right side and to account for a residual series resistance to the sensing contact.

Wheras the electrical network has a relative small number of devices to simulate the active area, the thermal grid is extended over the whole substrate. For that purpose, a quadratic grid of size $n \times m$ is used, expanded in each direction by additional resistors of the in n_{ext} rows and m_{ext} columns. Due to symmetry of the problem, again only one half of the substrate has to be computed. The thermal grid is finally enclosed by resistors representing the heat flow from glass to air $R_{\text{glass}-\text{air}}$.

In contrast to the electrical grid which is solely two-dimensional, we use multiple layers of the two-dimensional thermal grid for the representation of the glass substrate. These layers are vertically connected by additional thermal resistors, thus creating a three-dimensional thermal grid. In Fig. C.12, a cross-section is schematically shown. The left, upper, and right side of the substrate has contact to air,

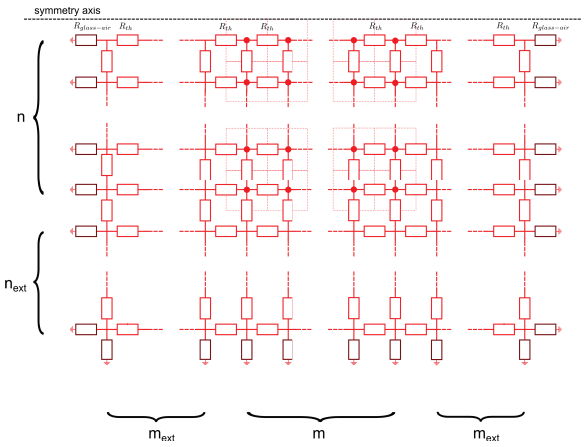

FIGURE C.11. Plane view of the thermal network used in the SPICE simulation representing the 4-wire crossbar measurement. Due to the symmetry of the setup (assuming no resistance of the metal), one half of the device is simulated and results are reflected afterwords at the symmetry axis. Big red dots represent the connection to a thermistor.

represented by the thermal resistors $R_{\mathrm{glass-air}}$. The bottom side of the substrate is in contact to a copper block, represented by the thermal resistors $R_{\mathrm{glass-Cu}}$. However, the latter are assumed to be zero, realizing an ideal heat transition from glass into the copper block, due to the use of thermal heat paste (cf. Fig. A.5b).

Altogether, the electrical and the thermal grid consists of around 44000 devices. A further increase of the network is limited by the computing time, reaching already several hours. For advanced simulations, finite-element models have to be developed with grids which can be meshed most densely where the thermistor array is connected. This will be the topic of further studies. Nevertheless, such a network model is easy to built and to solve with freely available software and thus a simulation is possible for anybody.

Thermal resistors representing the heat flow are calculated by

$$R_{\mathrm{th}} = \frac{d}{\alpha_{\mathrm{glass}} A}\,, \tag{4}$$

where d is the characteristic length between two nodes, A is the area through which the heat flows, and α_{glass} is the heat conductivity of glass. The thermal resistors representing a heat transition e.g. from glass to air are calculated by

$$R_{\mathrm{th,glass-air}} = \frac{1}{\alpha_{\mathrm{glass-air}} A}\,. \tag{5}$$

Furthermore, the power dissipation generated by a current flowing through the ITO electrodes is incorporated by an additional heat flow into the thermal network. Since a certain power is coupled out by light, we consider this by reducing the amount of heat generated within the OLED by 20%.

Please note that α_{glass} is a heat conductivity, whereas $\alpha_{\mathrm{glass-air}}$ is a heat transition coefficient. All parameters used for simulation are summarized in Tab. 1.

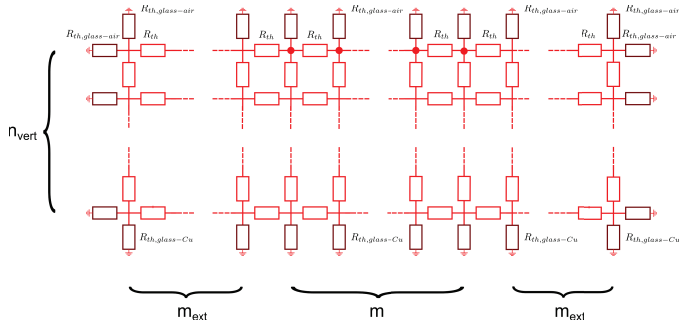

FIGURE C.12. Cross-section of the thermal network used in the SPICE simulation representing the 4-wire crossbar measurement. Multiple layers are linked vertically, realizing a 3D thermal grid to simulate the glass substrate. The heat flow from glass to air is simulated by complementary resistors at the outside of the glass substrate with values corresponding to the heat transition from glass to air or to heat transition from glass to copper. Big red dots represent the connection to a thermistor.

parameter	value
sheet resistance R_{sh}	$26.5\,\Omega$
series resistance R_{S}	$25\,\Omega$
activation energy E_{act}	$8\,\mathrm{k_B T_a}$
reference current I_{ref}	$3.942\,\mathrm{V}$
reference voltage V_{ref}	$1\,\mathrm{mA}$
exponent power law	8.7
power outcoupled as light n_{ext}	20%
heat conductivity glass α_{glass}	$1.8\,\mathrm{W/m/K}$
heat transfer coefficient glass to air $\alpha_{\mathrm{glass-air}}$	$10\,\mathrm{W/m^2/K}$

TABLE 1. Parameters used in the simulation of the 4-wire crossbar measurement setup.

Appendix D. Tabola lighting panel

A picture of the Tabola lighting panel can be found in Fig. D.13. It is produced by Fraunhofer COMEDD (Dresden, Germany) and uses a white OLED on an active area of 15 cm × 7.5 cm. Light is emitted through the 0.7 mm thick substrate glass. The top electrode acts as a reflector for enhanced light outcoupling. The Tabola lighting panel uses a glass encapsulation to prevent the materials from degradation. Connection of the metallic top electrode (cathode) to the power supply is realized at the four corners of the lighting panel. The ITO electrode (anode) is connected via a metallic frame all around the active area. Outside the active area both electrodes are separated by insulating layers.

Figure D.13. Picture of the Tabola lighting panel used in this work with a 15 cm × 7.5 cm large active area.

More information have been released for a transparent Tabola lighting panel in the world wide web: web-document of a transparent Tabola lighting panel.

Appendix E. Network model for simulation of an opaque Tabola

The SPICE model of the Tabola is similar to the network used for the 4-wire measurement. Due to the vertical and horizontal symmetry of the lighting panel, one quarter is simulated and reflected afterwards. Furthermore, the metallic electrode (opaque) as well as the ITO electrode (transparent) are modeled by an electrical grid, representing the sheet resistance. The sheet resistance of the ITO is set to 12.5 Ω (as measured) and the sheet resistance of the metal is set to a 100 times smaller value. The ITO electrode is connected to a highly conductive metal frame along all edges of the lighting panel. The metal electrode is connected at each corner, ca. 2 cm along the short side and 1 cm along the longer side. The electrical grid is adjusted accordingly. In areas where both electrodes overlap outside the active area, they are fabricated with a separating insulating layer.

The luminance values are calculated from the local current density. We fit the experimental values for the dependency of current efficiency (CE) over current density at total currents (< 500 mA) where a high brightness homogeneity is ensured. This can be seen in Fig. E.16. For the computation of luminance data from the simulation results, the computed current density and fitted relation between luminance and current density below is used.

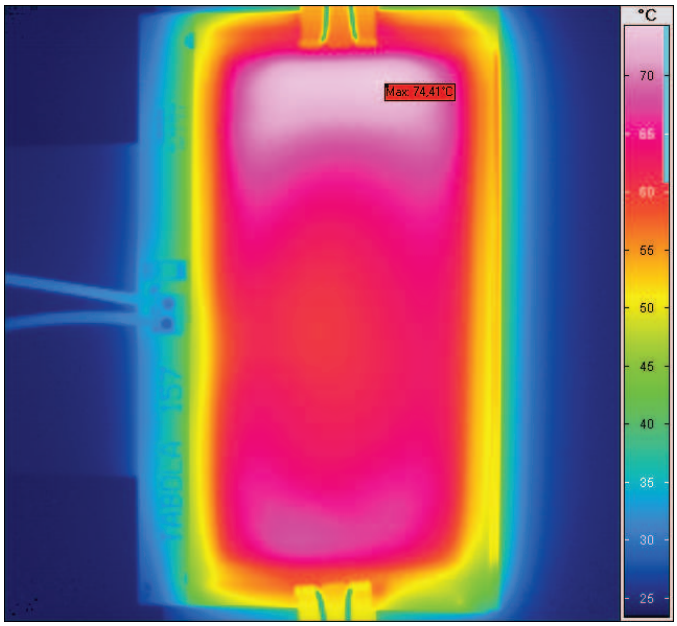

FIGURE D.14. Thermal imaging of the Tabola at a current of 1 A. The highest temperature is ca. 75 °C which does not lead to a significant degradation of the lighting panel. However, by applying higher currents, degradation starts and the hottest regions will show a reduced luminance.

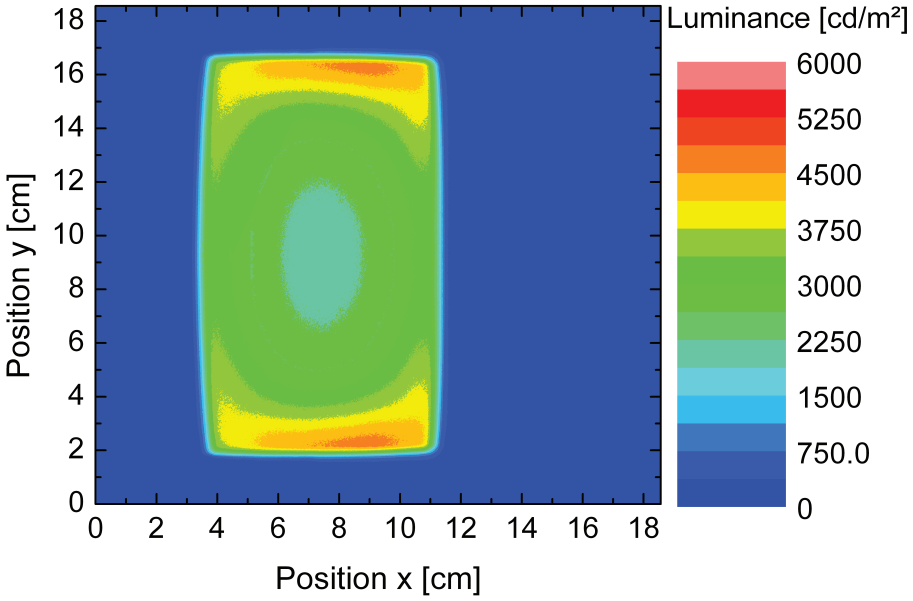

FIGURE D.15. Luminance imaging of the Tabola at a current of 1 A. The central region has a brightness of 2000 cd/m^2, whereas the brightest regions show values up to 6000 cd/m^2. Such a brightness inhomogeneity is clearly visible.

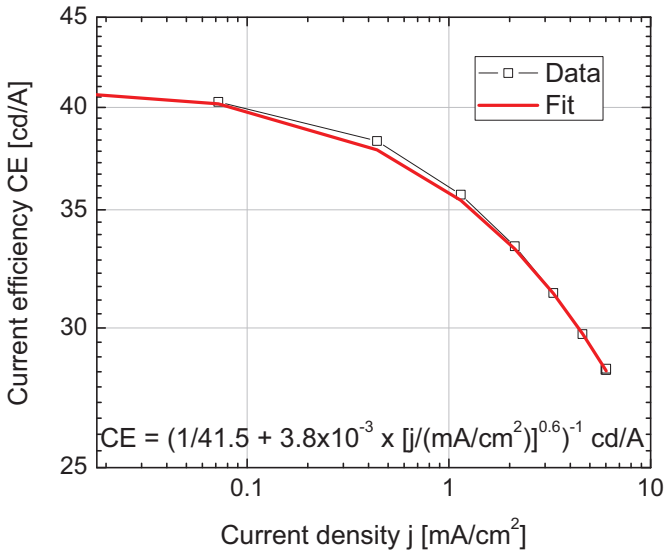

FIGURE E.16. Fit of the function between current efficiency and current density to calculate the luminance from the simulation result.

References

[1] K. T. Kamtekar, A. P. Monkman, M. R. Bryce, Recent advances in white organic light-emitting materials and devices (WOLEDs), Adv. Mater. 22 (5) (2010) 572–582.

[2] B. Geffroy, P. le Roy, C. Prat, Organic light-emitting diode (OLED) technology: materials, devices and display technologies, Polymer International 55 (6) (2006) 572–582.

[3] Y.-S. Tyan, Organic light-emitting-diode lighting overview, Journal of Photonics for Energy 1 (1) (2011) 011009–011009.

[4] S. Reineke, F. Lindner, G. Schwartz, N. Seidler, K. Walzer, B. Lüssem, K. Leo, White organic light-emitting diodes with fluorescent tube efficiency, Nature 459 (7244) (2009) 234–238.

[5] Press release LG Chem 2013/04/10.

[6] K. Neyts, M. Marescaux, A. U. Nieto, A. Elschner, W. Lovenich, K. Fehse, Q. Huang, K. Walzer, K. Leo, Inhomogeneous luminance in organic light emitting diodes related to electrode resistivity, J. Appl. Phys. 100 (11) (2006) 114513–4.

[7] J. Park, J. Lee, Y.-Y. Noh, Optical and thermal properties of large-area OLED lightings with metallic grids, Org. Electron. 13 (1) (2012) 184–194.

[8] M. Slawinski, M. Weingarten, M. Heuken, A. Vescan, H. Kalisch, Investigation of large-area OLED devices with various grid geometries, Organic Electronics 14 (10) (2013) 2387–2391.

[9] Y.-S. Tsai, S.-H. Wang, C.-H. Chen, C.-L. Cheng, T.-C. Liao, Using copper substrate to enhance the thermal conductivity of top-emission organic light-emitting diodes for improving the luminance efficiency and lifetime, Appl. Phys. Lett. 95 (23) (2009) 233306–3.

[10] S. Chung, J.-H. Lee, J. Jeong, J.-J. Kim, Y. Hong, Substrate thermal conductivity effect on heat dissipation and lifetime improvement of organic light-emitting diodes, Appl. Phys. Lett. 94 (25) (2009) 253302–3.

[11] J. Park, H. Ham, C. Park, Heat transfer property of thin-film encapsulation for OLEDs, Org. Electron. 12 (2) (2011) 227–233.

[12] L. Yang, B. Wei, J. Zhang, Transient thermal characterization of organic light-emitting diodes, Semiconductor Science and Technology 27 (10) (2012) 105011–.

[13] A. A. Zakhidov, S. Reineke, B. Lüssem, K. Leo, Hydrofluoroethers as heat-transfer fluids for OLEDs: Operational range, stability, and efficiency improvement, Organic Electronics 13 (3) (2012) 356–360.

[14] H. Sasabe, J. Kido, Multifunctional materials in high-performance OLEDs: Challenges for solid-state lighting, Chem. Mater. 23 (3) (2010) 621–630.

[15] C. Gärditz, A. Winnacker, F. Schindler, R. Paetzold, Impact of joule heating on the brightness homogeneity of organic light emitting devices, Appl. Phys. Lett. 90 (10) (2007) 103506–3.

[16] A. W. J. Gielen, M. Barink, J. van den Brand, A. M. B. Van Mol, The electro-thermal-mechanical performance of an OLED: A multi-physics model study, in: Thermal, Mechanical and Multi-Physics simulation and Experiments in Microelectronics and Microsystems, 2009. EuroSimE 2009. 10th International Conference on, 2009, pp. 1–6.

[17] X. Qi, S. R. Forrest, Thermal analysis of high intensity organic light-emitting diodes based on a transmission matrix approach, J. Appl. Phys. 110 (12) (2011) 124516–11.

[18] M. Slawinski, D. Bertram, M. Heuken, H. Kalisch, A. Vescan, Electrothermal characterization of large-area organic light-emitting diodes employing finite-element simulation, Org. Electron. 12 (8) (2011) 1399–1405.

[19] L. Pohl, E. Kollár, A. Poppe, Z. Kohri, Nonlinear electro-thermal modeling and field-simulation of OLEDs for lighting applications I: Algorithmic fundamentals, Microelectronics Journal 43 (9) (2012) 624–632.

[20] P. Schwamb, T. C. Reusch, C. J. Brabec, Passive cooling of large-area organic light-emitting diodes, Organic Electronics 14 (8) (2013) 1939–1945.

[21] A. Fischer, P. Pahner, B. Lüssem, K. Leo, R. Scholz, T. Koprucki, K. Gärtner, A. Glitzky, Self-heating, bistability, and thermal switching in organic semiconductors, Phys. Rev. Lett. 110 (12) (2013) 126601–.

[22] M. Shaw, N. Yildirim, Thermal and electrothermal instabilities in semiconductors, Vol. Volume 60, Academic Press, 1983, pp. 307–385.

[23] E. Schöll, Nonequilibrium Phase Transitions in Semiconductors, Springer, Berlin Heidelberg, 1987.

[24] L. Pohl, E. Kollar, Extension of the SUNRED algorithm for electrothermal simulation and its application in failure analysis of large area (organic) semiconductor devices, in: Thermal Investigations of ICs and Systems (THERMINIC), 2011 17th International Workshop on, 2011, pp. 1–6.

[25] R. Meerheim, R. Nitsche, K. Leo, High-efficiency monochrome organic light emitting diodes employing enhanced microcavities, Appl. Phys. Lett. 93 (4) (2008) 043310–3.

[26] C. Weichsel, S. Reineke, M. Furno, B. Lüssem, K. Leo, Organic light-emitting diodes for lighting: High color quality by controlling energy transfer processes in host-guest-systems, J. Appl. Phys. 111 (3) (2012) 033102–7.
[27] A. U. Keskin, A simple analog behavioural model for NTC thermistors including selfheating effect, Sensors and Actuators A: Physical 118 (2) (2005) 244–247.
[28] A. Fischer, P. Pahner, B. Lüssem, K. Leo, R. Scholz, T. Koprucki, J. Fuhrmann, K. Gärtner, A. Glitzky, Self-heating effects in organic semiconductor crossbar structures with small active area, Organic Electronics 13 (11) (2012) 2461–2468.
[29] G. Schwartz, S. Reineke, K. Walzer, K. Leo, Reduced efficiency roll-off in high-efficiency hybrid white organic light-emitting diodes, Appl. Phys. Lett. 92 (5) (2008) 053311–3.
[30] N. C. Giebink, S. R. Forrest, Quantum efficiency roll-off at high brightness in fluorescent and phosphorescent organic light emitting diodes, Phys. Rev. B 77 (23) (2008) 235215–.
[31] S.-J. Su, E. Gonmori, H. Sasabe, J. Kido, Highly efficient organic blue-and white-light-emitting devices having a carrier- and exciton-confining structure for reduced efficiency roll-off, Adv. Mater. 20 (21) (2008) 4189–4194.
[32] C. Murawski, K. Leo, M. C. Gather, Efficiency roll-off in organic light-emitting diodes" (in press) (adma201301603), Adv. Mater.